PERGAMON

International Journal of Heat and Mass Transfer 45 (2002) 1045–1054

International Journal of HEAT and MASS TRANSFER

www.elsevier.com/locate/ijhmt

Identification of furnace thermal characteristics from resistance measurements

J.P. Garandet *, C. Salvi

DTA/CEREM/DEM/SPCM/LSP, Centre d'Etudes Nucleaires Grenoble, Commissariat à l'Energie Atomique, 17 rue des Martyrs, F-38054 Grenoble Cedex 9, France

Received 26 May 2001; received in revised form 26 June 2001

Abstract

A brief review of existing diagnostic methods allowing to determine the interface position and velocity during the solidification of liquid metals and semiconductors is first presented. We then show that a recently proposed electronic design can be used to measure the electrical resistance of the sample with a very high accuracy: the peak to peak noise on the signal is significantly lower than 1 μΩ. In the tin-based system used in our investigations, this amounts to a resolution in terms of solid–liquid interface position of the order of a few micrometers. The experimental results show that our resistance measurement technique allows to identify the thermal lag of the furnace in the initial solidification stage, as well as a transfer function between actual and imposed interface fluctuations.

1. Introduction

In the field of material sciences, it is now well accepted that the implementation of in situ diagnostics maximises the scientific return of the experiments, by providing useful informations on the growth conditions. More specifically, one of the key issues in the directional solidification problem is the measurement of the position and velocity of the growth interface. In transparent materials, direct observation of the solid–liquid front is possible by optical means. The morphology and the velocity of the growth front can thus be accurately characterised, see e.g. [1,2]. Unfortunately, application oriented materials such as semiconductors and metals are opaque to natural light, and optical techniques cannot be applied directly. Transparent models, such as succinonitrile or pivalic acid, can to some extent be representative of the properties of liquid metals, but a perfect adequation is of course impossible.

An interesting alternative allowing the implementation of optical diagnostics in opaque materials is the use of a transparent facility. In this field, interesting results were obtained by Alkemper et al. [3] on aluminium alloys directionally solidified within an aerogel furnace. Aerogels are transparent materials of extremely low thermal conductivity 0.02 W/m K, made of nanometer size silica spheres, that can be used as crucible. The authors were able to determine on line the brightness – or equivalently the temperature – of the sample surface from a CCD camera. This allowed to valuably monitor the thermal field and the growth velocities of the alloys.

A natural extension of optical techniques in opaque materials is the use of X-rays. As the absorption coefficient in a given material is proportional to its mass density, a solid–liquid interface can thus be visualised. Image magnifications of up to 800 were achieved by the development of new technologies [4], but the adaptation of standard non-destructive testing facilities may be sufficient in some cases [5]. However, the limitations of X-ray optics are such that the technique is not as accurate as natural light methods. Nevertheless, in the case of gallium, a change of density upon melting of only 3% was found to be sufficient to obtain valuable informations regarding interface shape [5].

Another interesting possibility is the use of ultrasonic vibrations: it was shown that the motion of the growth

* Corresponding author. Tel.: +33-476-883663; fax: +33-476-885117.

E-mail address: garandet@chartreuse.cea.fr (J.P. Garandet).

0017-9310/02/$ - see front matter
PII: S0017-9310(01)00207-1

Nomenclature

a	sample radius (m)
C_p	sample heat capacity (J/kg K)
e	heat transfer barrier thickness (m)
f_1, f_2	cut-off frequencies of the second-order low pass filter (Hz)
G	furnace temperature gradient (K/m)
h	heat transfer coefficient (W/m^2 K)
H	non-dimensional heat transfer coefficient
I	input current or resistance measurement (A)
J	non-dimensional adiabatic zone thickness
K	thermal conductivity (W/m K)
L	length of temperature gradient zone (m)
L_T	pulling length (m)
r_1, r_2	potentiometer resistances (Ω)
R	sample resistance (Ω)
S	sample cross-section (m^2)
T_H, T_C	temperature in hot and cold zones (K)
T_M	melting temperature (K)
$V(t)$	actual interface velocity (m/s)
V_0	prescribed pulling velocity (m/s)
W	non-dimensional latent heat

Greek symbols

α	sample thermal diffusivity (m^2/s)
φ	furnace cooling rate (J/s)
ρ	sample density (kg/m^3)
ρ_E	sample resistivity (mΩ)
τ	furnace thermal lag (s)
ΔH	solidification latent heat (J/kg)
ΔT_I	solidification kinetic undercooling (K)

Subscripts

C	cold zone
H	hot zone
L	liquid phase
S	solid phase

front could be tracked through the implementation of an emission/detection system based on a piezo-ceramic transducer [6]. Indeed, as the acoustic impedances of the solid and liquid phases differ, an ultrasonic pulse will be reflected at the interface. The resolution is of the order of 15 μm, and the beauty of the ultrasound technique is that it can be used on both electrically conducting and electrically insulating materials.

Last but not least, interesting informations regarding interface position and or velocity can be obtained based on the fact that most materials exhibit a significant change in resistivity upon melting. This is specially true for semiconductors, since some of them (for instance Si, Ge, GaSb and InSb) become metallic in the liquid phase. Variations of the solid fraction and of the overall resistance of the sample can thus be correlated. For instance, a resistance technique was used to follow experimentally the variations of the liquid fraction within the mushy zone in aqueous solutions of sodium nitrate [7]. Similarly, in single phase growth of metals and alloys, the variations of the overall resistance of the sample can be used to monitor the motion of the solid–liquid interface.

Our purpose in this work is to show that a differential resistance measurement technique can be implemented to yield the interface position with an accuracy of a few micrometers in metallic alloys, which represents a significant improvement with respect to all the diagnostic techniques previously mentioned. We shall see that it becomes possible to follow the motion of the solid–liquid interface during the early stages of solidification and to identify a transfer function between actual and imposed interface fluctuations. Such data is interesting from a process control standpoint, but it can also be used as benchmark to validate numerical simulations of the heat transfer phenomena within the furnace. We shall first in Section 2 recall the basis of the differential resistance measurement technique, presented in detail in an earlier paper [8], as well as some background on furnace characteristics. The presentation of the experimental results will be carried out in Sections 3 and 4 will be devoted to a discussion of the heat transfer phenomena within the furnace based in part on existing numerical models.

2. Background

2.1. Differential measurement technique

Our experimental arrangement is an original Bridgman type furnace pictured in Fig. 1. It features two solid–liquid interfaces, one allowed to move for solidification and melting, the other maintained at a fixed position to be used as reference. This configuration has been developed in our laboratory in the frame of the Mephisto microgravity programme, see e.g. [9]. The classical measurement technique is straightforward. A stabilised current of typical intensity Im and pulsation ω, respectively, ranging typically from 10 to 100 mA and 100 to 1000 rad/s goes through the sample. The overall resistance R of the sample can be measured using a standard four probes technique. Assuming the system to be radially homogeneous, R can be expressed as:

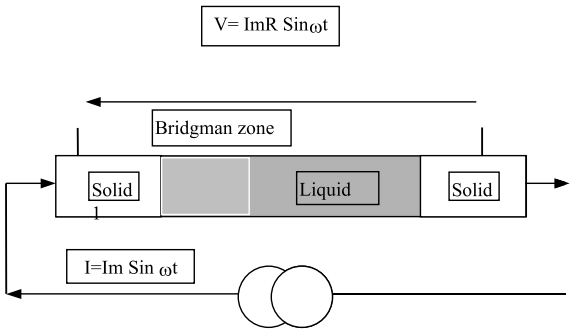

Fig. 1. General measurement design.

$$R = \left(\int_A^B \rho_E(z)\,dz \right) \Big/ S. \quad (1)$$

The points A and B represent the extrema points along the current path, taken here to be in the z-direction, ρ_E and S standing, respectively, for the sample electrical resistivity and cross-section. From an accuracy standpoint, such an integrating technique is clearly a limitation. Let us take for instance a metallic alloy of global resistance 20 mΩ; a typical 10^{-4} accuracy measurement then allows to obtain the true value with an error of less than 2 μΩ. Now the resistance variations due to actual interface motion in the Bridgman zone may be much lower, say of the order of 1 mΩ. We thus find that the relative accuracy on this variation is only of 2×10^{-3}. The idea of the differential measurement technique is to directly access this 1 mΩ variation, so that, keeping the same 10^{-4} accuracy, it becomes possible to limit the uncertainty to 0.1 μΩ.

The key step is to realise a differential measurement between the two halves of the sample. As shown in Fig. 2, an electrode is inserted in the liquid zone to allow access to the partial emfs $V1$ and $V2$, $V1$ representing the resistance that evolves with the motion of the interface and $V2$ the reference resistance corresponding to the fixed interface. A differential transformer can then be used to extract the emf V_S, given as

$$V_S = \alpha(V1 - V2), \quad (2)$$

where α being a proportionality constant depending on the transformer. The maximum sensitivity, allowing to detect the smallest resistance variation, will be obtained for initially perfectly symmetrical samples, $V1 = V2$. As this condition may not be easily met in practice – one may clearly be interested in carrying out measurements at various locations in the Bridgman zone – it is interesting to introduce a control parameter. Our choice was to add one potentiometer in series with the inductances at the transformer primary, and to connect the measurement electrode to the cursor of the potentiometer since it can be shown that the potentiometer resistances $r1$ and $r2$ can be used to set V_S to zero [8]. The overall sketch of the measurement technique is summarised in Fig. 3, where the various symbols appearing respectively represent: V_S the emf measured at the secondary, L_S the inductance at the secondary, M_S the coupling between primary and secondary, $L1$ and $L2$ the inductances on both sides of the electrode at the primary, $r1$ and $r2$ the potentiometer resistances on both sides of the electrode at the primary, $V1$ and $V2$ (resp. $R1$ and $R2$) the emfs (resp. the sample resistances) on both sides of the electrode at the primary.

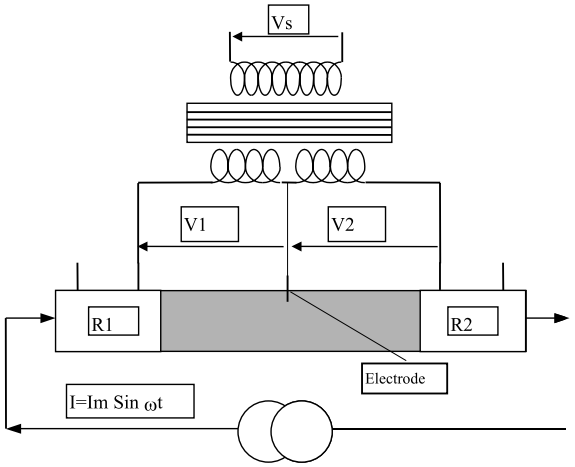

Fig. 2. Differential measurement technique: principle.

The design was tested with a short circuited output to characterise its noise spectral density. Typical values for the various impedances were $L1 = L2 = 50$ mH. A spectral analyser HP 35670A was used for the

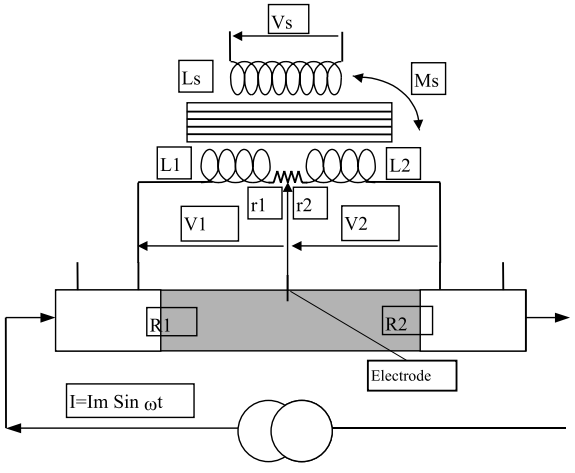

Fig. 3. Differential measurement technique featuring control resistances.

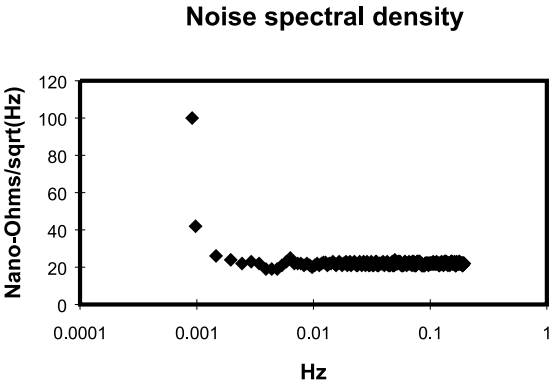

Fig. 4. Characterisation of the low temperature spectral noise density.

measurements. The curve shown in Fig. 4, taken for an input current $I = 20$ mA, clearly exhibits a plateau at about 20 nΩ/Hz, extending towards very low frequencies (0.001 Hz). Such a feature is clearly interesting for directional solidification experiments, since the relevant frequencies for the heat and mass transport processes are generally very small, of the order of 0.1 Hz or less [10]. With such a measurement accuracy, equivalent peak-to-peak variations in the (0–1 Hz) bandwidth should thus be less than 0.1 μΩ. Even in good conductors such as metals where the measurement sensitivity is limited, this amounts to an uncertainty in terms of interface position in the micrometer range [8]. It should be noted that a fivefold increase of the input current to $I = 100$ mA will result in a fivefold decrease of the noise power spectral density, but that higher values of I may be associated with perturbing Joule effects.

2.2. Furnace characteristics

In the Bridgman technique where solidification or fusion is initiated by a relative displacement of the sample and the thermal field of the furnace, the solid–liquid interface does not react immediately. Two factors can explain the difference between the actual interface velocity and its prescribed value. First, some time is necessary for the temperature information to proceed longitudinally and radially from the furnace to the sample via the containment crucible and/or various thermal barriers. In the case of conduction limited transport, an often realistic assumption in the case of metallic materials, characteristic time scales for these processes can usually be written as L^2/α, L and α, respectively, representing the relevant length and the medium heat diffusivity. However, even if the information transmission is very fast, actual and prescribed interface velocities will not necessarily be equal: indeed, the cooling rate φ is necessarily limited. One can build for such a mechanism a characteristic kinetics time scale given as $\Delta Q/\varphi$, ΔQ being the heat amount that needs to be extracted. We shall come back in some detail on both mechanisms in the discussion of Section 4. In any case, from an empirical standpoint, the initial interface velocity transient following a sudden impulse can often described as (see e.g. [11–13]):

$$V(t) = V_0[1 - \exp(-t/\tau)], \tag{3}$$

where V and V_0, respectively, represent the actual and prescribed growth velocities, τ standing for the thermal lag time of the furnace. Integrating the above expression from the start of the pulling phase at $X = 0$ and $t = 0$, we get

$$X(t) = V_0 t - V_0\tau[1 - \exp(-t/\tau)]. \tag{4}$$

The difference between actual and prescribed interface positions increases exponentially over a time scale τ from zero to $V_0\tau$. Similarly, at the end of the pulling phase, assuming that the same thermal lag period is necessary for the interface to stop, the actual interface velocity is given as

$$V(t) = V_0 \exp(-t/\tau). \tag{5}$$

Allowing for a change of co-ordinate origins, $X = 0$ and $t = 0$ now representing the end of the pulling phase, integration of Eq. (8) from $X = 0$ and $t = 0$ yields

$$X(t) = V_0\tau[1 - \exp(-t/\tau)]. \tag{6}$$

After a long enough stabilisation period, $X = V_0\tau$, and it can be seen that the interface catches up for the recoil of the initial transient.

The validity of this simple model, which assumes the relative interface and furnace thermal profiles to be the same at various locations in the solidification zone when the steady-state is reached, can be tested using our differential resistance measurement. Similarly, our diagnostic technique allows to discuss the response of a given furnace to periodic fluctuations of the growth conditions in terms of heat transfer kinetics between furnace, containment crucible and metallic sample. It is the purpose of the experimental work we shall now present to identify a globally coherent model of the furnace behaviour.

3. Experimental results

3.1. Procedure

As mentioned earlier, our experiments were carried out in a double gradient Bridgman furnace, allowing for the existence of a reference fixed interface. The temperature gradients are imposed by means of a sodium heat pipe on the hot end and a water cooled heat extractor on the cold end. The hot and cold zones are separated by a 3 mm thick adiabatic region. Solidifica-

tion and melting are induced by an imposed motion of this thermal unit, the sample containing crucible being maintained at a fixed position. The heat flow can be assumed to be one-dimensional in the interface region, whereas the isotherms are certainly significantly curved near the input of the hot and cold ends. The starting material was 6 N grade tin, the samples were 4 mm in diameter and circa 1 m long; they were contained in a 2 mm thick silica glass crucible. An important problem that needed to be addressed concerns the uniformity of the liquid vein diameter. Indeed, the tolerances necessary to fit the solid state feed in the crucible at room temperature were found to result in an incomplete filling in the liquid region during the experiment. In order to avoid free surfaces and to guarantee an uniform cross-section path for the electrical current, the crucible has an open end in the middle, which serves as a reservoir of raw material.

All the experiments presented in the frame of this work were carried out with the same maximum (furnace) temperature of $T_H = 500$ °C, the temperature in the cold zone being of the order of $T_C = 20$ °C, leading to a temperature gradient on the liquid side of the interface of circa 200 K/cm. Pulling velocities for solidification and fusion were varied from 0.6 to 20 mm/min. As for the translation length L_T, it is in principle only limited by the geometrical dimension of the setup. However, at high L_T, the average sample temperature is modified, which renders the interpretation of the resistance signals more difficult. In practice, we kept L_T between 20 and 100 mm, most experimental results being obtained at 40 and 50 mm.

Our choice of tin as working material is not based on the facility of diagnostic implementation, since the sensitivity of the measurement is limited due to the high electrical conductivity of the material. It thus appeared all the more interesting to show that our resistance diagnostic could provide useful information on the heat transfer phenomena within the furnace even in challenging conditions. Another key issue with tin is to find an electrode stable enough to withstand operation on a long period. Preliminary tests using graphite or tungsten as electrode material were not fully successful. Fortunately, rhenium was found to be totally inert with liquid tin, and no drift was observed on the resistance signal for a time span of more than one month. It should be kept in mind that an adaptation of our measurement technique to higher temperature liquid metals or semiconductors depends on the possibility to find a stable enough electrode, which may be quite difficult in some cases.

3.2. Indicial response

In this series of experiments, solidification and fusion stages were carried out, a stage being defined as the succession of a translation and a stabilisation period. The procedure for conversion of resistance to position is as follows: after a prescribed furnace translation L_T, we wait long enough for a steady-state to be reached, and scale both the resistance and position signals from their maximum–minimum difference. We thus obtain a proportionality relationship between resistance and position variations of the form

$$\Delta z = \xi \Delta R. \tag{7}$$

As shown in [8], the proportionality constant ξ can be approximately related to the liquid and solid state resistivities of the material, as well as to the sample cross-section. In any case, this procedure allows to compare the experimental results with the predictions of Eqs. (4) and (6). A typical raw experimental result is shown in Fig. 5, the length and prescribed velocity of this solidification stage being respectively, 40 mm and 10 mm/min; as expected, the furnace position initially increases linearly with time, whereas a lag in terms of interface position, as deduced from the resistance measurement, is clearly apparent. Taking the difference between the resistance and position signals, we find that the system behaves exponentially as predicted by Eq. (4), with a thermal lag constant of 30 s. Similarly, at the end of the pulling phase, the return to steady-state conditions is also exponential, as predicted by Eq. (6), and the same thermal lag constant $\tau = 30$ s allows to perfectly fit the experimental data.

More details regarding this solidification stage are apparent in Fig. 6, where the same result is presented on a larger scale. An interesting feature is that the resistance values are not exactly the same at the beginning and at the end of the solidification/stabilisation stage. As the overall sample temperature is slightly modified due to the interface motion, such a feature is not unreasonable: as a matter of fact, the overall resistance is slightly lower at the end of the stage since the solid is a better conductor than the liquid. Also apparent in Fig. 6 is the

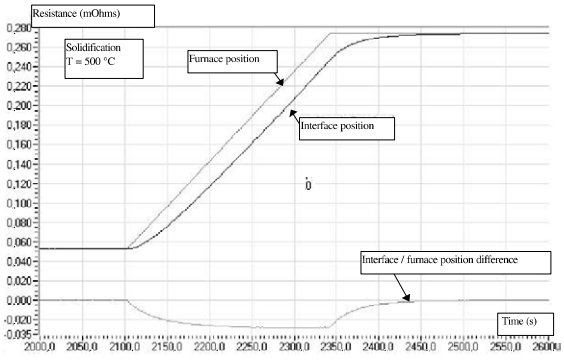

Fig. 5. Respective furnace and interface positions, along with their difference, as a function of time.

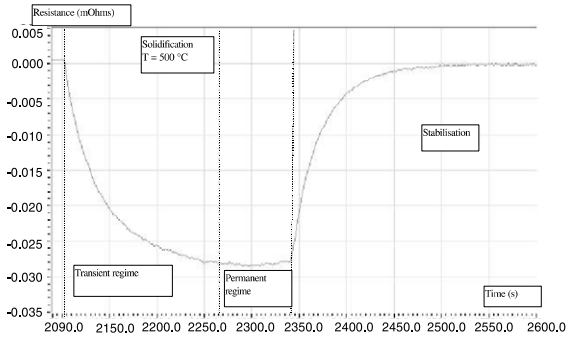

Fig. 6. Resistance signal in the initial and steady-state regimes, followed by a stabilisation period.

remarkable stability of the resistance signal after the stabilisation period, with peak-to-peak noise values below 0.2 μΩ.

Summarising all our results, we found the exponential behaviour predicted from Eqs. (4) and (6) to be observed in all stages. Moreover, for a given stage, we found that the thermal lag constants of the translation (solidification or fusion) and the stabilisation were indeed equal, the maximum difference never exceeding one second. Generally, the thermal lags of the fusion stages were somewhat lower, say between 24 and 27 s than their solidification stage counterparts, that could always be well fitted with $\tau = 30$ s. Possible reasons accounting for such a difference will be discussed below.

3.3. Periodic excitation

In this series of experiments, the effect of imposed small amplitude (typically ±1 mm) periodic motion of the furnace was characterised. Representative signals for furnace position and resistance signals are shown in Fig. 7. It can be again remarked that the peak-to-peak noise on the resistance signal is again very small, allowing an accurate processing of the experimental information. Both the amplitude and phase shift of interface motion were found to be independent of the amplitude of furnace motion. Such a result, associated to the behaviour of the system subject to sudden variations of the growth rate, led us to present the relation between input and output (furnace and interface motion) in the form of a linear filter. The frequency range investigated extended from 1.6×10^{-4} to 0.125 Hz. Below 10^{-3} Hz, furnace motion is slow enough for the interface to follow the imposed variations. The amplitude of the resistance signal is constant and the phase shift very close to zero. A significant behaviour change is observed in the frequency range 6×10^{-3} Hz, which corresponds to a characteristic time scale in the 24–30 s span, as identified from the indicial response experiments.

Upon subsequent increase of the frequency of the applied variations, the amplitude of the resistance signal keeps on decreasing, and the phase shift takes values below 90°. This indicates that the system is not a simple first-order low pass filter, as might have been deduced from indicial response experiments, but that higher cut-off frequencies are necessarily present. Indeed, the curve shown in Fig. 8(a) clearly shows that the amplitude of the experimental resistance data can be very well fitted using a second-order low pass filter of cut-off frequencies $f_1 = 5.9 \times 10^{-3}$ Hz and $f_2 = 0.2$ Hz. The lowest cut-off frequency $f_1 = 5.9 \times 10^{-3}$ Hz, corresponding to a time scale $\tau = 27$ s, was taken as imposed for the sake of consistency with the indicial response experiments, but f_2 was taken as a free parameter to be fitted from the experiments. The agreement is not so good regarding phase shifts (see Fig. 8(b)), but the second-order low

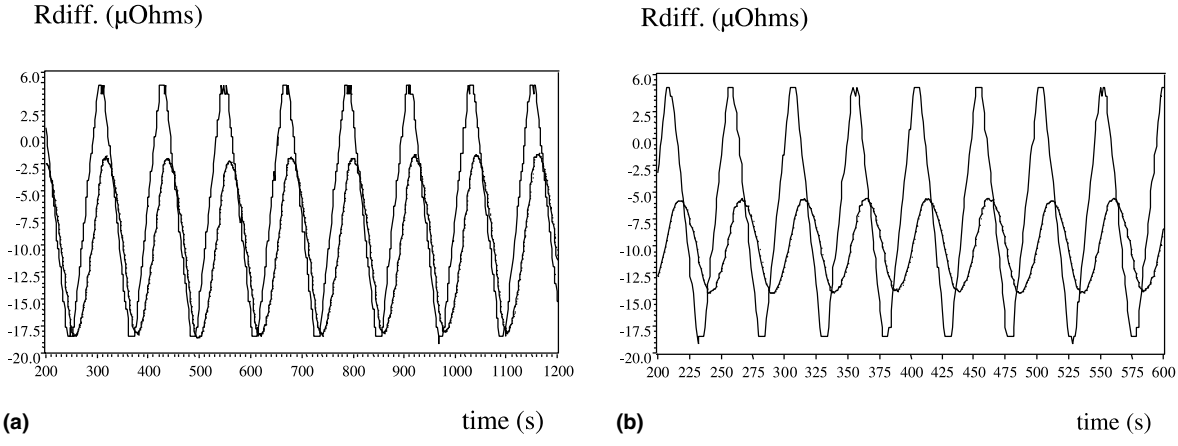

Fig. 7. Typical furnace and resistance signals in periodic excitation experiments. The frequency of the imposed furnace motion is 8.2 mHz (a) and 20 mHz (b).

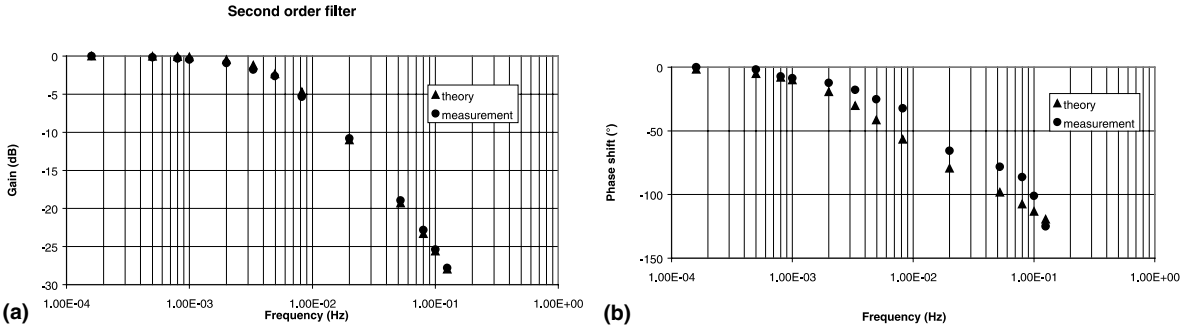

Fig. 8. Comparison in terms of amplitude (a) and phase shift (b) of the experimental results with the predictions from a second-order low pass filter of cut-off frequencies $f_1 = 5.9 \times 10^{-3}$ Hz and $f_2 = 0.2$ Hz.

pass filter representation still provides a satisfying representation of the data.

4. Discussion

A first conclusion of the indicial response experiments is that the identified thermal lag constant depends only weakly on the starting point, length, direction and pulling velocity of the various stages. Such a finding indicates that the thermal field in our thermal unit is fairly reproducible from one experiment to another. In general terms, one should keep in mind that the heat transfer phenomena in the furnace a priori depend on the relative location of the sample and heating/cooling subsystems with respect to the sample. The relative uniformity of τ in our experiments is a tribute to the adequate conception of the experimental device.

An interpretation of our indicial response solidification experiments can be based on the numerical results of Fu and Wilcox [11]. In these simulations, heat exchange from the sample to its surroundings is modelled through hot zone and cold zone transfer coefficients, the temperatures of these hot and cold zones being inputs of the problem. The temperature gradient is only established in a short adiabatic region, such as is the case in our experimental configuration. The formulation is only one-dimensional, but so is the output of our resistance diagnostic that represents an average over the sample cross-section. A number of test cases were simulated, with varying growth velocities, heat transfer coefficients in the hot and cold zones, length of adiabatic region and latent heat were carried out. The time lag between furnace isotherms and interface motion was found to be adequately accounted for by an expression of the form:

$$\tau = \rho_L C_p a / \underline{h}\eta, \tag{8}$$

where ρ_L, C_p, a, respectively, represent the liquid phase mass density, the heat capacity and the radius of the sample, $\underline{h}$ standing for the geometric mean of the hot and cold zones heat transfer coefficients. As for η, it is an empirical expression relating the growth parameters, coming from a fit of the numerical results, given as:

$$\eta = 3.55 \exp[-(1.12W^{1/2} + 0.077J + 1.69JH + 0.018JW)]. \tag{9}$$

The non-dimensional parameters W, J and H appearing in the above expression are defined as follows:

- $W = \Delta H / C_p(T_H - T_C)$, ΔH being the latent heat of solidification;
- $J = l_a/a$, l_a being the length of the adiabatic zone;
- $H = \underline{h}a/K_L$, K_L being the liquid phase thermal conductivity of the sample.

The difficulty in applying such a model lies in the estimation of the heat transfer coefficients. In our experimental device, various thermal barriers between the sample and the furnace can be identified:

1. Between the outer surface of the sample and the inner surface of the crucible. The gap necessary to fit the sample within the crucible before the experiments is about 0.1 mm thick. It only exists in the cold zone, where it is filled with 200 mbar Argon. The liquid is assumed to completely fill the crucible in the hot zone (see Section 3.1).
2. Across the 2 mm thick silica glass crucible.
3. Between the outer surface of the crucible and the inner surface of the furnace. The gap necessary to move the furnace along the sample–crucible system is about 0.2 mm thick. It exists in both the hot and cold zones, and is filled with atmospheric air.

It should be stated that these gap thicknesses should be taken as estimates, and we are definitely not in a position to account for the roughness of the surfaces [14]. Nevertheless, to the first-order, the cold and hot zones' heat transfer coefficients can be taken as:

$$1/h_C = e_{Argon}/K_{Argon} + e_{Silica}/K_{Silica} + e_{Air}/K_{Air}, \tag{10}$$

$$1/h_H = e_{Silica}/K_{Silica} + e_{Air}/K_{Air}. \tag{11}$$

Plugging in physical constants taken from the Handbooks, $K_{Argon}(20\ ^\circ C) = 0.018$ W/m K, $K_{Air}(20\ ^\circ C) = 0.026$ W/m K, $K_{Air}(500\ ^\circ C) = 0.056$ W/m K [15],

$K_{\text{Silica}}(20\ ^\circ\text{C}) = 1.5$ W/m K, $K_{\text{Silica}}(500\ ^\circ\text{C}) = 2$ W/m K [16], we get $h_C \approx 70$ W/m^2 K, $h_H \approx 220$ W/m^2 K, $\underline{h} = (h_C h_H)^{1/2} \approx 120$ W/m^2 K and $H \approx 0.008$. The other non-dimensional parameters appearing in eq. (9) are the normalized adiabatic zone thickness $J = 1.5$ and latent heat, which can be estimated from $\Delta H = 6 \times 10^4$ J/kg, $C_p = 250$ J/kg K [17] to be $W = 0.5$. Using these values in Eq. (9), we find $\eta = 1.4$. The last parameter necessary for the derivation of τ in Eq. (8) is the liquid phase mass density that we took equal to $\rho_L \approx 7000$ kg/m^3 [17]. We finally obtain $\tau \approx 21$ s, a value that compares favourably with the experimental observations. Indeed, looking for a better agreement would be illusory in our opinion in view of the numerous simplifying assumptions of the model. Besides, from an experimental standpoint, we are not in a position to accurately characterize the roughness of the surfaces in contact, that could be an important feature to be checked [14] if we were looking for more accurate results.

It should be mentioned that there exist other numerical models of the heat transfer phenomena during initial transients in Bridgman solidification (see e.g. [18,19]). However, their applicability to our experimental configuration and growth conditions is questionable. For instance, in [18], the temperature gradient is established all along the sample and is thus not restricted, as in our furnace, to a short adiabatic zone. Another shortcoming of the simulations of [18] – at least regarding the interpretation of our experimental data – is that the latent heat generated at the growth front is very large. Heat conservation at the solidification interface can be written as

$$K_S G_S = K_L G_L + \rho_S \Delta H V, \tag{12}$$

where K_S, G_S, K_L, G_L, respectively, represent the thermal conductivities and the temperature gradients in the solid and liquid phases, V standing for the instantaneous growth velocity. In our experimental conditions, $\rho_S \Delta H V$ is only a small fraction (20% at the most) of the conduction fluxes, a situation typical of metals. On the other hand, in [18], the simulations pertain to cases where $\rho_S \Delta H V$ is at least twice as high as $K_L G_L$, a situation relevant for poorly conducting materials such as semiconductors and weak thermal gradients. Consequently, the estimation of the decay time proposed in [18], namely

$$\tau = \rho_S \Delta H l_S / 2 K_S G_S, \tag{13}$$

where l_S represents the length of the solid at the beginning of growth, cannot be expected to be valid for the analysis of our results. Apart from these physical considerations, the numerical constant estimated from Eq. (9) is not in agreement with our data: estimating l_S as $l_S \approx (T_M - T_C)/G_S$ and plugging in our growth conditions $(T_M - T_C) \approx 200$ K, $G_S \approx 10^4$ K/m and material parameters $\rho_S \approx \rho_L \approx 7000$ kg/m^3, $\Delta H \approx 6 \times 10^4$ J/kg, $K_S \approx 60$ W/m K [17], we get $\tau \approx 7$ s a value too small compared with our observations.

The applicability of the simulations of [19] to our experimental conditions was a priori more promising, since the ratios of the latent heat contribution to the diffusive flux are of the same order of magnitude. However, the underlying hypothesis in [19] is that there are no lateral heat exchanges between the sample–crucible system and the furnace environment, solidification being induced by a programmed cooling, a situation quite different from our experimental configuration. The delay in interface motion was identified in [19] with the kinetics of heat transfer along the sample, $\tau \approx l^2/\alpha$, l being the length of the established temperature gradient and α the thermal diffusivity of the sample, taken equal in the solid and liquid phases in [19]. The numerical application to our experimental configuration, taking $l = l_S + l_L \approx 0.03$ m and an average thermal diffusivity $\alpha \approx 3 \times 10^{-5}$ m^2/s, would yield $\tau \approx 30$ s, in very close agreement with our experimental data. However, our opinion is that such an agreement should be considered as coincidental in view of the large differences between the numerical model and the experimental system.

We did not find in the literature papers dealing with the simulation of the transient heat transfer in melting configuration, so that no definite conclusion regarding the difference in terms of thermal lags between solidification and melting stages can be drawn. However, the model of [11] can again be invoked to propose a tentative explanation. Indeed, solidification requires that more heat is extracted from the cold zone, whereas fusion requires more heat to be transmitted from the hot zone. Even though the final results are summarized in [11] with an average heat transfer coefficient between the hot and cold zones, it can be thought that cold (resp. hot) zone heat transfer will have a stronger influence on the process kinetics in solidification (resp. fusion) cycles. As the heat transfer coefficient is smaller in the cold zone than in the hot zone (mostly due to the lower thermal conductivity of the surrounding gases), it follows that the thermal lag time can be expected to be higher for solidification stages, as observed in practice.

Another mechanism can also be invoked to explain the observed difference: the driving force necessary for the solidification to proceed can in principle induce a significant delay in the process. In a pure metal like tin solidifying with a non-faceted interface, the kinetic undercooling is expected to be proportional to the growth velocity

$$\Delta T_I = \gamma V_0 \tag{14}$$

the proportionality constant γ being of order of magnitude 10^4 when expressed in K s/m. This kinetic undercooling translates in a time lag on the interface motion that can be expressed as:

$$\Delta t = \Delta T_I/(G_S V_0) = \gamma/G_S, \quad (15)$$

where G_S stands for the temperature gradient on the solid side of the interface. Plugging in our measured value $G_S = 10^4$ K/m, we find that the kinetic undercooling could account for a time lag in the second range. It is thus a likely mechanism to be invoked to explain, at a given pulling velocity V_0, the higher time lags observed in solidification stages, since no kinetic undercooling is expected in the fusion process. However, a quantitative assessment would require the proportionality coefficient γ to be accurately known, which is unfortunately not the case. As a matter of fact, there is no consensus in the literature regarding the growth mode (dislocation assisted vs continuous) at low undercoolings [20], and the relationship between ΔT and V_0 could be more complex than what has been stated in Eq. (14). In any case, even though it may be an important variable of the problem, kinetic undercooling is probably not sufficient to explain the observed difference between solidification and fusion stages.

Regarding our periodic furnace oscillations experiments, we did not find simulation results available in the literature for comparison. One of the reasons may be the absence of reference experimental data that can be used to validate the models: classical measurement techniques, such as inserting a thermocouple within the sample, are clearly too perturbative. It is only from in situ measurements, such as our resistance diagnostic, that a clean information can be obtained. All that can be stated in this paper is that the experimental results could be adequately accounted for in the form of a second-order low pass filter, both in terms of amplitude and phase shift. An apparent paradox is thus that the indicial response of the system points towards first-order behaviour, whereas the harmonic excitation procedure led to the identification of two cut-off frequencies.

However, one should keep in mind that, in indicial response experiments, the higher cut-off frequency is expected to influence the signal only in the very beginning of the growth process. On a time scale of a few τ, the time resolution is not high enough for such details to be apparent. Nevertheless, it is satisfying the lower cut-off frequency is consistent with the thermal lag time as defined in Eq. (3), since the heat transfer phenomena between the sample and its surroundings are essentially the same. As for the higher cut-off frequency, it could perhaps be related to radial diffusive heat transfer kinetics across the sample. All that can be said at this point is that dedicated numerical simulations would be necessary to draw a definite conclusion.

Another problem still unclear concerns the high frequency behaviour of our thermal system, as the existence of still higher cut-off frequencies cannot be excluded. In practice however, it is the lowest cut-off frequency that governs the kinetics of the heat transfer processes and as such is the most important for solidification. Similarly, the linearity assumption regarding the transport phenomena within the furnace is certainly questionable from a theoretical standpoint, but our data show that a linear representation is adequate in experimental practice. To sum up things, ours is a case where simplistic empirical approaches are probably sufficient, even though the reality is clearly more complex.

5. Concluding remarks

Our purpose in this work was to show that an high accuracy resistance measurement technique allows to obtain valuable informations on heat transfer phenomena in solidification. We found that even in high temperature furnaces the method can be used to track the growth interface position with an accuracy of a few micrometers. Our approach in this work has been mostly empirical, but our data could also be used to validate a thorough numerical modelling of the heat transfer phenomena in the furnace.

Indicial response experiments, where the solid–liquid interface has to react to a sudden variation of the pulling rate, demonstrated that the response of the system was exponential, the characteristic furnace lag time being of the order of 27 s. An interpretation of the transient kinetics of the solidification process was proposed, based on the simulation results of Fu and Wilcox [11] that pertain to a growth configuration close to ours. In our experimental device, the process kinetics are likely to be limited by the various thermal barriers between the sample and the furnace, rather than by latent heat extraction.

The effect of periodic variations of the furnace position was found to be adequately accounted for in the form of a second-order low pass linear filter in the Fourier space. The smallest cut-off frequency of this filter is in very good correspondence with the lag time identified from the indicial response experiments. This means that even though simple first-order models are not physically correct, they may be fruitfully used in a variety of cases. However, the prediction of the amount of solute segregation resulting from fluctuating interface velocities [21] requires the full transfer function to be accounted for.

Future lines of work include the application of the technique to other solidification problems, such as the detection of gaseous species in the liquid phase. From a technical standpoint, the adaptation of the measurement technique to standard, single gradient, furnace configuration is currently under way with support from the European Space Agency and the Centre National d'Etudes Spatiales.

Acknowledgements

The present work has been carried out within the frame of the Gramme agreement between the Cnes and the Cea. It is a pleasure to thank A. Borgis, A. Kehrli and T. Oresic for their technical assistance. Numerous fruitful discussions on the topic with Dr. P. Lehmann are also gratefully acknowledged.

References

[1] S. Akamatsu, G. Faivre, T. Ihle, Symmetry broken double fingers and seaweed patterns in thin film directional solidification of a non faceted cubic crystal, Phys. Rev. E 51 (1995) 4751–4773.

[2] M.E. Glicksman, M.B. Koss, E.A. Winsa, Dendritic growth velocities in microgravity, Phys. Rev. Lett. 73 (1994) 573–576.

[3] J. Alkemper, S. Sous, C. Stöcker, L. Ratke, Directional solidification in an aerogel furnace with high resolution optical temperature measurements, J. Crystal Growth 191 (1998) 252–260.

[4] P.A. Curreri, W.F. Kaukler, Real time X-ray transmission microscopy of solidifying AlIn alloys, Metall. Mater. Trans. A. 27 (1996) 801–808.

[5] T.A. Campbell, J.N. Koster, Visualization of liquid–solid interface morphologies in gallium subject to natural convection, J. Crystal Growth 140 (1994) 414–425.

[6] M. Schmachtl, A. Schievenbusch, G. Zimmermann, W. Grill, Crystallization process control during directional solidification in a high temperature gradient furnace by guided ultrasonic waves and real time signal evaluation, Ultrasonics 36 (1998) 291–295.

[7] T.G.L. Shirtcliffe, H.E. Huppert, M.G. Worster, Measurement of the solid fraction in the crystallization of a binary melt, J. Crystal Growth 113 (1991) 566–574.

[8] C. Salvi, J.P. Garandet, A novel resistance measurement technique in the field of directional solidification, Rev. Sci. Inst. 72 (2001) 255–262.

[9] J.J. Favier, A. Rouzaud, J. Comera, Influence of various hydrodynamic regimes in a melt on a solidification interface, Rev. Phys. Appl. 22 (1987) 713–718.

[10] J.P. Garandet, J.J. Favier, D. Camel, Segregation phenomena in crystal growth from the melt, in: D.T.J. Hurle (Ed.), Handbook of Crystal Growth, North-Holland, Amsterdam, 1994.

[11] T.W. Fu, W.R. Wilcox, Rate change transients in Bridgman–Sockbarger growth, J. Crystal Growth 51 (1981) 557–567.

[12] C.A. Wang, A.F. Witt, J.R. Carruthers, Analysis of crystal growth characteristics in a conventional vertical Bridgman configuration, J. Crystal Growth 66 (1984) 299–308.

[13] J.J. Favier, P. Lehmann, B. Drevet, J.P. Garandet, D. Camel, S.R. Coriell, A study of morphological stability during directional solidification of a Sn–Bi alloy in microgravity, in: L. Ratke et al. (Eds.), Lecture Notes in Physics, vol. 464, Springer, Berlin, 1996, pp. 77–94.

[14] S.M.S. Wahid, C.V. Madhusudana, Gap conductance in contact heat transfer, Int. J. Heat Mass Transfer 43 (2000) 4483–4487.

[15] R.E. Bolz, G.L. Tuve (Eds.), Handbook of Tables for Applied Engineering Science, second ed, CRC Press, Boca Raton, 1972.

[16] Y.S. Touloukian, C.Y. Ho (Eds.), Thermophysical Properties of Matter, TRPC Data Series, vol. 2, IFI Plenum, 1973.

[17] C.J. Smithells, in: E.A. Brandes, G.B. Brooks (Eds.), Smithells Metals Reference Book, seventh ed., Butterworth–Heinemann, London, 1992.

[18] M. Saitou, A. Hirata, Numerical calculation of two-dimensional unsteady solidification problem, J. Crystal Growth 113 (1991) 147–156.

[19] C. Stelian, T. Duffar, J.L. Santailler, I. Nicoara, Influence of temperature oscillations on the interface velocity during Bridgman crystal growth, J. Crystal Growth (in press).

[20] J.J. Favier, Etude des cinétiques de cristallisation par application de l'effet thermoélectrique, analyse de la température d'une interface de solidification, Ph.D. thesis, Grenoble University, 1977.

[21] F.Z. Haddad, J.P. Garandet, D. Henry, H. Ben Hadid, Analysis of the unsteady segregation in crystal growth from a melt. I. Fluctuating interface velocity, J. Crystal Growth 204 (1999) 213–223.